Available online at www.sciencedirect.com
SCIENCE DIRECT®
Scripta Materialia 52 (2005) 1181–1186
Scripta MATERIALIA
www.actamat-journals.com

Finite element simulations of dynamic strain ageing effects at V-notches and crack tips

S. Graff [a,*], S. Forest [a], J.-L. Strudel [a], C. Prioul [b], P. Pilvin [c], J.-L. Béchade [d]

[a] Centre des Matériaux/UMR 7633, Ecole des Mines de Paris/CNRS, BP 87, 91003 Evry, France
[b] MSSMAT, Ecole Centrale Paris, Grande Voie des Vignes, 92295 Châtenay-Malabry, France
[c] IUP Lorient, Université de Bretagne Sud, 2, rue Le Coat St-Haouen, 56325 Lorient, France
[d] SRMA, CEA Saclay, 91191 Gif sur Yvette, France

Available online 13 March 2005

Abstract

Finite element simulations of PLC effects in notched and CT (compact tensile) specimens of aluminium alloys are presented, based on a macroscopic PLC constitutive model. They predict the formation and propagation of intense strain rate localization bands. In particular, the predicted size of the plastic zone around the crack tip in a pre-cracked CT specimen is compared to the value found when using a standard elastoplastic model neglecting PLC effects.

Keywords: Portevin–Le Châtelier effect; Dynamic strain ageing; Crack tip; Finite element simulations

1. Introduction

The Portevin–Le Châtelier effect (PLC) effect is the manifestation of dynamic strain ageing (DSA). This effect is associated with negative strain rate sensitivity (SRS) [1]. It is characterized by the presence of stress serrations on the macroscopic load/displacement curve in constant strain rate tests or strain bursts in constant stress rate tests [2]. These serrations are associated with the multisite initiation and propagation of strain rate localization bands. Such phenomena are shown experimentally in the polycrystalline Al–Cu alloy in [3]. A multiscale modelling approach for polycrystal plasticity is used to model jerky flow in the Al–Mg polycrystals in [4]. For the sake of simplicity, however, these engineering materials are usually modeled by constitutive elastoplastic equations, that do not take these strain or strain rate localization phenomena into account. A frequent claim for doing that is that, contrary to flat tensile specimens, the complex geometry of real components induces stress concentrations and generates non-uniform strain fields which tend to absorb and/or disperse strain localization events. The main objective of this work is to examine this argument by means of finite element simulations in the case of V-notched and CT specimens.

In a previous work [5], PLC effects and Lüders band propagation have been simulated in flat and U-notched specimens of different curvature radii using the phenomenological model proposed in [6]. The numerical results are in good agreements with experimental results obtained for an Al–Cu alloy and a mild steel. In the present work, finite element simulations are performed to predict the response at V-notches and at a crack tip in a pre-cracked CT specimen. For the same material, two models are compared: a standard von Mises elastoplastic model that neglects DSA effects, on the one hand, and the PLC model taken from [6], on the other hand. Attention is drawn on the comparison of plastic zone sizes in both cases.

* Corresponding author. Tel.: +33 1 60 763046; fax: +33 1 60 763150.
E-mail address: stephanie.graff@ensmp.fr (S. Graff).

1359-6462/$ - see front matter © 2005 Published by Elsevier Ltd. on behalf of Acta Materialia Inc.
doi:10.1016/j.scriptamat.2005.02.007

2. The macroscopic model of strain ageing

The constitutive model presented in [6] is available to simulate instabilities in materials, containing interstitial or substitutional elements that can segregate at dislocations and lock them. It can be used to simulate both the PLC effect and the Lüders behavior, as shown in [5]. The evolution equations try to mimic the mechanisms of repeated breakaway of dislocations from their solute clouds and recapture, for instance, by mobile solutes. The total deformation is the sum of elastic and plastic strains

$$\underset{\sim}{\varepsilon} = \underset{\sim}{\varepsilon}^{\mathrm{e}} + \underset{\sim}{\varepsilon}^{\mathrm{p}}, \quad \underset{\sim}{\sigma} = \underset{\approx}{\mathbf{C}} : \underset{\sim}{\varepsilon}^{\mathrm{e}} \tag{1}$$

The tensor $\underset{\approx}{\mathbf{C}}$ is the fourth-rank tensor of elastic moduli. The yield criterion is

$$f(\underset{\sim}{\sigma}) = J_2(\underset{\sim}{\sigma}) - R \tag{2}$$

where J_2 is the second invariant of the stress tensor. The plastic flow rule is deduced from the normality law

$$\dot{\underset{\sim}{\varepsilon}}^{\mathrm{p}} = \dot{p}\frac{\partial f}{\partial \underset{\sim}{\sigma}}, \quad \dot{p} = \dot{\varepsilon}_0 \exp\left(-\frac{E_{\mathrm{a}}}{k_{\mathrm{B}}T}\right)\sinh\left(\frac{\langle f(\underset{\sim}{\sigma})\rangle V_{\mathrm{a}}}{k_{\mathrm{B}}T}\right) \tag{3}$$

where $\dot{p}$ is the viscoplastic multiplier; $\dot{\varepsilon}_0$ is a constant; $\langle f(\underset{\sim}{\sigma})\rangle$ means the maximum of $(f(\underset{\sim}{\sigma}), 0)$; T is the absolute temperature; V_{a} is the activation volume; and E_{a} is the activation energy. In this study, strain hardening is assumed to be isotropic and includes also the strain ageing term $P_1 C_{\mathrm{s}}$

$$\begin{aligned} R &= R_0 + Q[1 - \exp(-bp)] + P_1 C_{\mathrm{s}}, \\ C_{\mathrm{s}} &= C_{\mathrm{m}}[1 - \exp(-P_2 p^{\alpha} t_{\mathrm{a}}^{n})] \end{aligned} \tag{4}$$

where R_0, Q, b, P_1, P_2, α and n are material parameters. C_{s} is the concentration of solute atoms segregating around the dislocations which are temporarily immobilized by extrinsic obstacles. C_{m} is the saturated concentration around the dislocations. The time dependence of this segregation process can be described by the "relaxation–saturation" kinetics of Avrami

$$\dot{t}_{\mathrm{a}} = \frac{t_{\mathrm{w}} - t_{\mathrm{a}}}{t_{\mathrm{w}}}, \quad t_{\mathrm{w}} = \frac{\omega}{\dot{p}} \tag{5}$$

The ageing time t_{a} is the time of the diffusion of the solute atoms towards or along the dislocations. The time t_{w} is the mean waiting time of dislocations, which are temporarily stopped by extrinsic obstacles. It depends on the plastic strain rate. The parameter ω is the increment of the plastic strain produced when all stopped dislocations overcome their obstacles.

The PLC model has been implemented in a finite element program [5]. The differential equations have been integrated at each Gauss point of each element using a Runge–Kutta method of fourth order with automatic time-stepping. The resolution method for global balance has been based on a Newton algorithm. The elements used in all presented simulations are 8-node quadratic elements with reduced integration under plane stress conditions.

Table 1
Parameters of the PLC model in the 2091 Al-Li alloy at −20 °C (after [7])

Parameters	Units	2091 Al–Li
R_0	MPa	320
Q	MPa	140
b	–	29
P_1	MPa (at.%)$^{-1}$	11
P_2	s^{-n}	3.91
ω	–	10^{-4}
α	–	0.44
n	–	0.33
E_{a}	eV	0.15
v_{a}	nm^3 (at.%)$^{-1}$	11
C_{m}	at.%	2
$\dot{\varepsilon}_0$	s^{-1}	10^{-5}

Two aluminium alloys are considered in the following finite element simulations:the Al–Cu alloy studied in [5], and the 2091 Al–Li alloy investigated in [7]. The material parameters of the PLC model identified from tensile tests on straight samples are to be found in [5] for the first alloy, and in Table 1 for the second one. In order to simulate the PLC effect, the initial value of t_{a} is set to zero (see Eq. (5)).

A standard von Mises elastoplastic model is also used in the following for comparison. It is obtained simply by suppressing the ageing term $P_1 = 0$ in Eq. (4), the remaining parameters being left unchanged.

3. PLC effects in V-notched specimens

The tensile deformation of flat specimens with two symmetric V-notches have been computed for two different angles: 60°-V-notches and 90°-V-notches. All the V-notched specimens are the same ligament size of 20 mm, and the same total length of 50 mm. All the tests have been simulated under a constant displacement rate such that the mean strain rate reached in the notched deformed zone is equal to $4 \times 10^{-4}\ s^{-1}$. Fig. 1 shows the overall normalized load/displacement curves. For comparison, the response of a straight specimen with a width of 20 mm is also given. For each specimen, two curves are provided: the one obtained with the PLC model, and the one obtained with the standard model. Two main differences arise. The stress level reached with the PLC model is higher than for the standard model. This is due to the suppression of the hardening component $P_1 C_{\mathrm{s}}$ in Eq. (4) for the standard model. The more significant difference is the presence of serrations after a certain amount of plastic strain on the curves simulated with the PLC model. The amplitude of the serrations

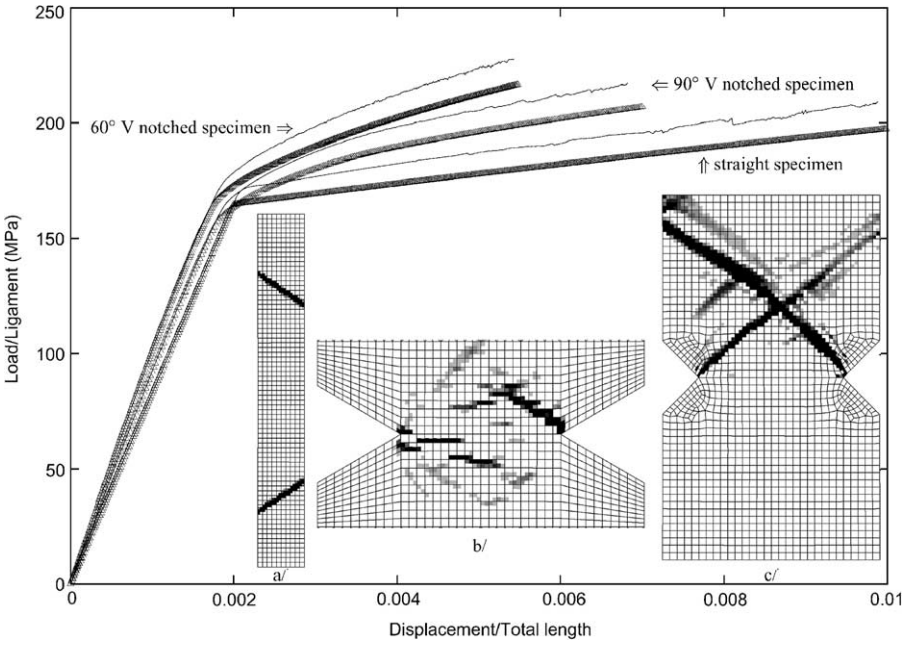

Fig. 1. Overall load/displacement curves for the tensile deformation of straight, 60° and 90°-V-notched specimens. The thick (resp. thin) curve is the result of the simulation with a standard (resp. PLC) model. The total length is 50 mm. Plastic strain rate maps at overall strain 0.0025 for: (a) straight specimens; (b) 60° V-notched specimen; (c) 90°-V-notched specimen. The black color corresponds to $\dot{p} > 0.2\%\ s^{-1}$.

is smaller in the 60°-V-notched specimen than in the 90°-V-notched specimen. The apparent yield stress for the 60°-V-notched specimen is larger than for the sharp 90°-V-notched specimen. This can be explained by a triaxiality effect [8].

Fig. 1 also shows maps of plastic strain rate $\dot{p}$ in the straight and notched samples. In the straight specimen, two strain rate localization bands start to develop simultaneously from an initial defect which has been numerically introduced. Then, they propagate through

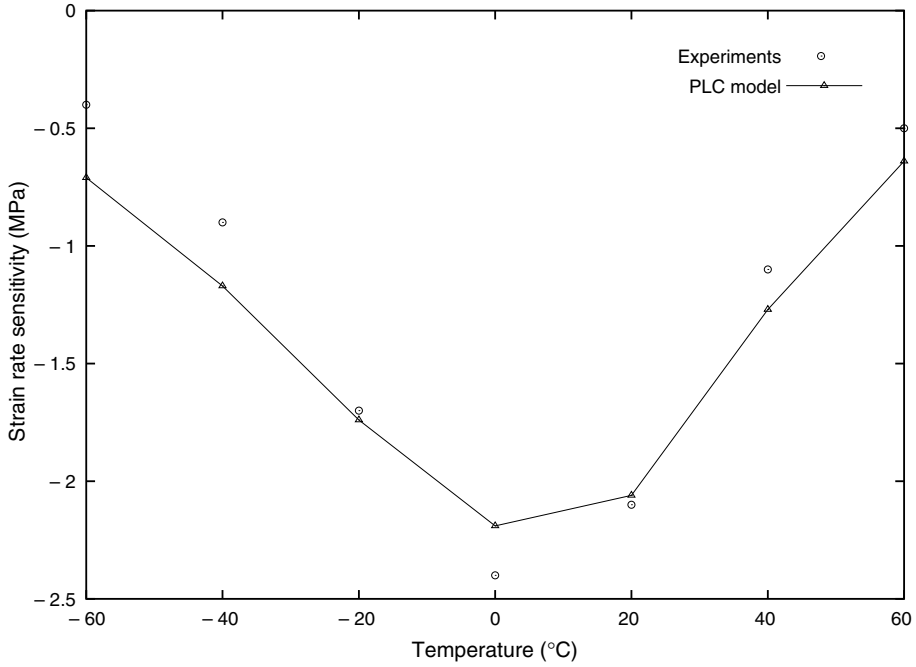

Fig. 2. Strain rate sensitivity as a function of temperature at 2% plastic strain: experimental results (after [7]) vs. numerical identification of the PLC model.

the whole specimen and are reflected at the top and bottom boundaries. One of them vanishes progressively, whereas the other one goes up and down at a constant speed. Each serration on the corresponding macroscopic curve is associated with the reflection of the band at one end of the specimen. In the case of V-notched specimens, the plastic strain rate bands start from the location of stress concentrations at the notches and propagate in the plastically deformed zone. They propagate on a short distance, disappear and new ones form starting from the notches. The plastic strain rate bands of the 60°-V-notched specimens remain confined in the region close to the ligament. In contrast, in sharp 90°-V-notched specimens, the intense strain rate bands extend far beyond the notched region. This feature can be related to the fact that the serrations on the overall curve of the 60°-V-notched specimen are less pronounced. Each band has been found to bring about 3% of plastic strain. The propagation of strain rate bands starts earlier (for a smaller overall plastic strain) in the 60°-V-notched specimen than in the 90°-V-notched specimen. This can be explained by a triaxiality effect [8].

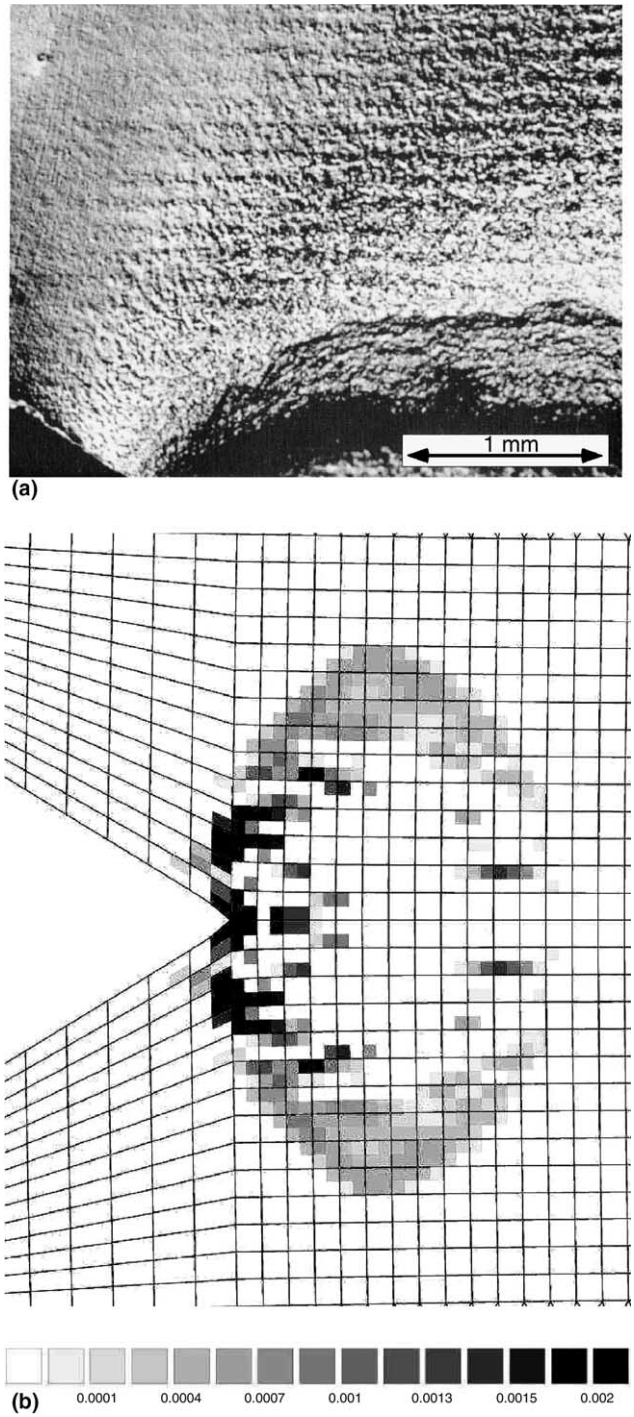

Fig. 3. (a) Micrograph obtained in Nomarski contrast near the notch tip of the 2091 Al–Li alloy specimen at −20 °C (after [7]). (b) Plastic strain rate (s^{-1}) map at relative displacement of the pins of 0.8 mm. The element size in the deformed zone is 150 μm. The unit of the color scale is s^{-1}.

It is possible to draw a qualitative comparison of the numerical results with the experimental ones presented in [7]. These authors investigated the influence of DSA on ductile tearing in the 2091 Al–Li alloy. This alloy exhibits a PLC effect at −20 °C during unixial deformation tests, which is associated with a depletion of the strain rate sensitivity (SRS). This effect is shown on Fig. 2 which gives the SRS as a function of the temperature at 2% of plastic strain. These results have been used to identify the material parameters of the PLC model for this alloys (see Table 1). For the identification over the considered temperature range, a temperature dependence of the activation volume V_a is introduced. It varies between 3 and 11 nm^3 (at.%)$^{-1}$. The authors in [7] used CT specimens without pre-cracking, with a 60°-V-notch and a ligament of 17.3 mm. Fig. 3 compares the experimental and simulated deformed zones at the notch. The specimen has been torn at −20 °C with a cross head velocity of 0.2 mm mn^{-1} to a crack extension of 3 mm. The existence of horizontal bands is evidenced. The simulated map represents the plastic strain rate $\dot{p}$ at a displacement equal to 0.4 mm. Horizontal strain rate bands in front of the crack tip are correctly predicted by the simulations. However, the band spacing depends on the mesh size which was set to 150 μm in the notched region.

4. PLC effects at a crack tip

Finite element simulations of the deformation behavior of a pre-cracked Al–Cu CT specimen have been performed for a ligament of 22 mm and 16 mm crack length. The main purpose of this part is to compare the plastic zone sizes obtained around the crack tip for the PLC and standard models. The mesh size at the crack tip is equal to 10 μm. Fig. 4 shows six maps comparing the PLC model and the standard model at two

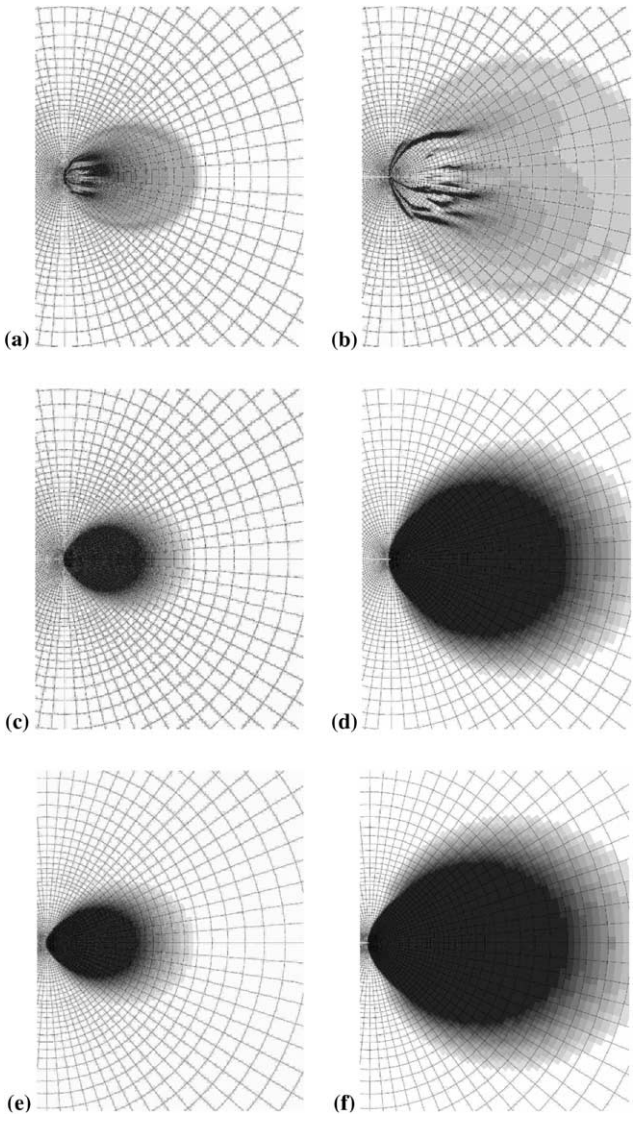

Fig. 4. Strain rate maps at the crack tip at relative pins displacements 0.07 mm (a) and 0.13 mm (b) for the simulation of a pre-cracked specimen with the PLC model. Plastic strain maps at the same displacements: simulations with the PLC model (c,d), and with a standard model (e,f). The color scale is the same as the Fig. 3. The unit for (a) and (b) is s^{-1} and the maps (c)–(f) are dimensionless.

different overall loadings: relative displacement of the pins of 0.07 mm and 0.13 mm. The maps (a) and (b) represent the PLC plastic strain rate fields $\dot{p}$. Multiple intense strain rate bands form at the crack tip and propagate in the plastic zone. The curvature of the observed bands is due to the strongly multiaxial stress field around the crack tip. On the map (b) each PLC plastic strain rate band brings about 2% plastic strain. The band spacing and band width are respectively equal to about 30 μm and 15 μm. The maps (c) and (d) represent the corresponding PLC plastic strain field at the same loading steps. They must be compared to the maps (e) and (f) obtained with the standard elastoplasticity model. Regions where the cumulative plastic strain p is less than 0.2% are in white. It turns out that both models lead to about the same plastic zone shape and size. This indicates that the very complicated and heterogenous propagation of strain rate bands takes place inside the same plastically deformed zone than for a standard model. The elliptical shape of the plastic zone in Fig. 4(c)–(f) are in agreement with the observations reported in [7].

5. Discussion and prospects

The following PLC effects arising in notched and cracked specimens have been evidenced in the previous simulations:

1. Serrations on the overall load/displacement curves are found for both 60° and 90°-V-notches. They are associated with the formation and propagation of multiple strain rate localization bands starting from the notches. These bands remain confined in the ligament zone in 60°-V-notched specimens and extend far beyond the ligament region in the case of 90°-V-notches. These results are similar to that found for U-notched specimens simulated and experimentally tested in [5]. The predicted horizontal bands in the deformed zone are in qualitative agreement with the experimental observations in [7].
2. Intense strain rate localization bands are produced at the crack tip in pre-cracked CT specimens. They are curved by the complex multiaxial stress state. The propagation of these intense strain rate bands does not affect the shape and the extension of the plastic zone, when compared to simulations with a standard elastoplastic model.

Complex strain localization phenomena take place at notches and crack tips in strain-ageing materials. Accordingly, neglecting them in the design of engineering components is not without consequence regarding failure assessment. Even though the plastic zone sizes predicted by the PLC and standard models are very close, the locally higher and strongly heterogeneous stresses associated with the PLC model may well play a significant role in the subsequent ductile fracture of the materials which has not been investigated here. This will be the subject of future analysis.

Acknowledgements

S. Graff and S. Forest thank L.P. Kubin (LEM/CNRS/ONERA, France) and D. Delafosse (Ecole des Mines de Saint-Etienne, France) for providing additional information about the results in [7] and for stimulating discussions.

References

[1] Kubin LP, Estrin Y. J Phys III 1991;1:929–43.
[2] Hänner P, Ziegenbein A, Rizzi E, Neuhäuser H. Phys Rev B 2002;65. 134109-1–20.
[3] Casarotto L, Tutsch R, Ritter R, Weidenmlliller J, Ziegenbein A, Klose F, et al. Comput Mater Sci 2003;26:210–8.
[4] Kok S, Bharathi MS, Beaudoin AJ, Fressengeas C, Ananthakrishna G, Kubin LP, et al. Acta Mater 2003;51:3651–62.
[5] Graff S, Forest S, Strudel J-L, Prioul C, Pilvin P, Béchade JL. Mater Sci Eng A, in press.
[6] Zhang S, McCormick PG, Estrin Y. Acta Mater 2000;49:1087–94.
[7] Delafosse D, Lapasset G, Kubin LP. Scr Metall Mater 1993;29:1379–84.
[8] Thomason PP. Ductile fracture of metals. Pergamon Press; 1990.